



# Blowout bifurcation and spatial mode excitation in the bubbling transition to turbulence

J.D. Szezech Jr.<sup>a</sup>, S.R. Lopes<sup>b</sup>, I.L. Caldas<sup>a</sup>, R.L. Viana<sup>b,\*</sup>

<sup>a</sup> Instituto de Física, Universidade de São Paulo, 05315-970, São Paulo, Brazil

<sup>b</sup> Departamento de Física, Universidade Federal do Paraná, Caixa Postal 19044, 81531-990, Curitiba, Paraná, Brazil

## ARTICLE INFO

### Article history:

Received 23 September 2010

Available online 8 October 2010

### Keywords:

Wave turbulence

Spatial mode excitation

Three-wave interaction

## ABSTRACT

The transition to turbulence (spatio-temporal chaos) in a wide class of spatially extended dynamical system is due to the loss of transversal stability of a chaotic attractor lying on a homogeneous manifold (in the Fourier phase space of the system), causing spatial mode excitation. Since the latter manifests as intermittent spikes this has been called a bubbling transition. We present numerical evidences that this transition occurs due to the so-called blowout bifurcation, whereby the attractor as a whole loses transversal stability and becomes a chaotic saddle. We used a nonlinear three-wave interacting model with spatial diffusion as an example of this transition.

© 2010 Elsevier B.V. All rights reserved.

## 1. Introduction

The idea that a low-dimensional chaotic attractor can generate turbulence out of a complex system like a fluid or plasma dates back to the seminal paper of Ruelle and Takens in the early 70s [1,2]. Numerical simulations of the onset of turbulence are usually performed in discrete lattices with time being a continuous or discrete variable, in oscillator chains and coupled map lattices, respectively [3]. In such spatially extended dynamical systems the concept of turbulence is closely related to the spatio-temporal chaos, which is characterized by chaotic temporal dynamics and decaying spatial correlations [4–6].

For spatially extended systems it is highly convenient to work in the Fourier phase space, wherein the state variables are the Fourier mode amplitudes generated by means of a pseudo-spectral decomposition of the original variables [7]. The dimensionality of this Fourier phase space is determined by the number of modes retained in the numerical simulation, and can be readily adjusted to match the needs of higher accuracy necessary to describe fully developed turbulence, for example [8]. On the other hand, since the onset of turbulence usually involves a few Fourier modes, the dimension can be substantially lower.

In the Fourier phase space, the scenario devised by Ruelle and Takens for the onset of turbulence can be described by a chaotic attractor lying on a low-dimensional homogeneous manifold embedded in the large-dimensional phase space of the system [1,2]. This manifold represents a spatially homogeneous and temporally chaotic subsystem [9,10]. The onset of spatio-temporal chaos occurs when part of the energy of the purely temporal mode is relayed to one or more spatial modes. After this transition the dynamics in the Fourier phase space explores directions transversal to the homogeneous manifold.

This description is particularly useful to clarify the role of the low-dimensional chaotic attractor in the generation of turbulence in spatially extended system [11,12]. In fact there must be a chaotic attractor embedded in the homogeneous manifold such that spatial modes be excited. The reason is that this chaotic attractor has an infinite number of unstable periodic orbits supporting the ergodic measure of the trajectories in the homogeneous manifold [13]. When one or more

\* Corresponding author.

E-mail address: [viana@fisica.ufpr.br](mailto:viana@fisica.ufpr.br) (R.L. Viana).

of such periodic orbits lose transversal stability (with respect to the homogeneous manifold) there is excitation of spatial modes. Since the dynamics driving such spatial mode excitation is chaotic, there follows that the spatial modes themselves will have their own chaotic evolution as well. Hence low-dimensional chaos becomes a necessary (albeit not sufficient) condition for spatial turbulence.

Just after the onset of turbulence, each time a spatial mode is excited a fast and narrow spike is produced for the corresponding Fourier amplitude. Since the onset of turbulence is followed by intermittent generation of spikes we called this phenomenon a bubbling transition [14–16]. Previously we showed that the intervals among these spikes follow the same universal scaling as of the so-called on-off intermittency [17,18]. In fact, in the context of spatially extended system, it is also known as in–out intermittency [19,20].

In this work we aim to investigate the scenario immediately following a bubbling transition in the directions transversal to the homogeneous manifold, which are the relevant directions when there is spatial mode excitation. The main point of this paper is to reveal which dynamical mechanisms in the homogeneous manifold drive specific features of the transversal dynamics, in particular when the manifold itself loses transversal stability *as a whole*. This situation has been identified as the so-called blowout bifurcation [21], and it is the mechanism underlying the bubbling transition in the class of spatially extended systems allowing a homogeneous invariant manifold where the dynamics is temporally chaotic.

The rest of this paper is organized as follows: Section 2 describes the three-wave interacting model and the Fourier mode expansion we make in order to work in the Fourier phase space. Section 3 considers the bubbling transition to spatio-temporal chaos exhibited by this model, focusing on the nonlinear excitation of spatial modes. Section 4 investigates the Lyapunov exponents of the model in order to obtain information on the blowout bifurcation as well as on the fluctuations of the Lyapunov exponents, when computed at finite time. Our Conclusions appear in the last section.

## 2. Spatially extended nonlinear three-wave model

In principle, the numerical technique of pseudo-spectral decomposition can be used to any nonlinear system of partial differential equations involving spatial and time derivatives. We have found that the bubbling transition to turbulence, which is the phenomenon we are interested in, is particularly well described in a nonlinear three-wave model with spatial diffusion. This system occurs in a plethora of problems in fluid dynamics [22,23], plasma physics [24,25] and nonlinear optics [26–28]; and is mathematically described by a system of coupled-mode nonlinear partial differential equations which exhibit complex behavior [29]. The nonlinear three-wave model describes the exchange of energy among a high-frequency (parent) wave and its sideband (daughters) with quadratic interactions, as well as with a spatial diffusion term [30–32].

The three dispersive monochromatic waves propagating along the  $x$ -direction have complex amplitudes denoted as  $A_\alpha$ ,  $\alpha = 1, 2, 3$ . Their wave numbers and frequencies must satisfy matching conditions for the triplet,

$$\mathbf{k}_3 = \mathbf{k}_1 + \mathbf{k}_2, \quad (1)$$

$$\Omega_{\mathbf{k}_3} = \Omega_{\mathbf{k}_1} + \Omega_{\mathbf{k}_2} - \delta, \quad (2)$$

where  $\delta$  is a small frequency mismatch, which was introduced since, even for perfectly matched wave vectors, the respective frequencies obtained from the linear dispersion relations may not be likewise matched.

From the specific linear dispersion relation, each wave can be assigned a group velocity  $v_{g\alpha} = d\Omega_{\mathbf{k}_\alpha}/dk_\alpha$ , which we assume satisfying the ordering  $v_{g2} > v_{g1} > v_{g3}$ . In this case  $A_1(x, t)$  stands for the parent wave amplitude,  $A_2(x, t)$  and  $A_3(x, t)$  being the corresponding amplitudes for the faster and slower daughter waves, respectively [29]. In a non-magnetized plasma, for example,  $A_1$  can be a transverse electromagnetic wave,  $A_2$  a ion-acoustic wave, and  $A_3$  is a Langmuir wave (anti-Stokes mode) [24,25].

We can introduce dissipation effects phenomenologically by adding growth and decay rates, such that the coefficients  $\nu_1 > 0$  and  $\nu_{2,3} < 0$  represent energy injection (through wave 1) and dissipation (through waves 2 and 3), respectively. Diffusion is also introduced by a Laplacian term in the parent wave, which provides a cutoff in the linear wave growth, being essential to nonlinear saturation [30]. We suppose that the nonlinearities in the wave interactions are sufficiently weak, such that only quadratic terms in the wave amplitudes need to be considered.

The equations governing the dynamics of the resonant three-wave interaction are [29,30]

$$\frac{\partial A_1}{\partial t} + v_{g1} \frac{\partial A_1}{\partial x} = A_2 A_3 + \nu_1 A_1 + D \frac{\partial^2 A_1}{\partial x^2}, \quad (3)$$

$$\frac{\partial A_2}{\partial t} + v_{g2} \frac{\partial A_2}{\partial x} = -A_1 A_3^* + \nu_2 A_2, \quad (4)$$

$$\frac{\partial A_3}{\partial t} + v_{g3} \frac{\partial A_3}{\partial x} = i\delta A_3 - A_1 A_2^* + \nu_3 A_3, \quad (5)$$

where  $D$  is a diffusion coefficient.

The group velocities, frequency mismatch, and diffusion coefficient take on fixed values:  $v_{g1} = 0.0$ ,  $v_{g2} = 1.0$ ,  $v_{g3} = -1.0$ ,  $\delta = 0.1$ , and  $D = 1.0$ , respectively, corresponding to the solitonic regime of Ref. [29]. The growth rate will be often kept fixed as  $\nu_1 = 0.1$ , and the decay rates  $\nu_2 = \nu_3$  are always negative, constituting the variable parameter in the

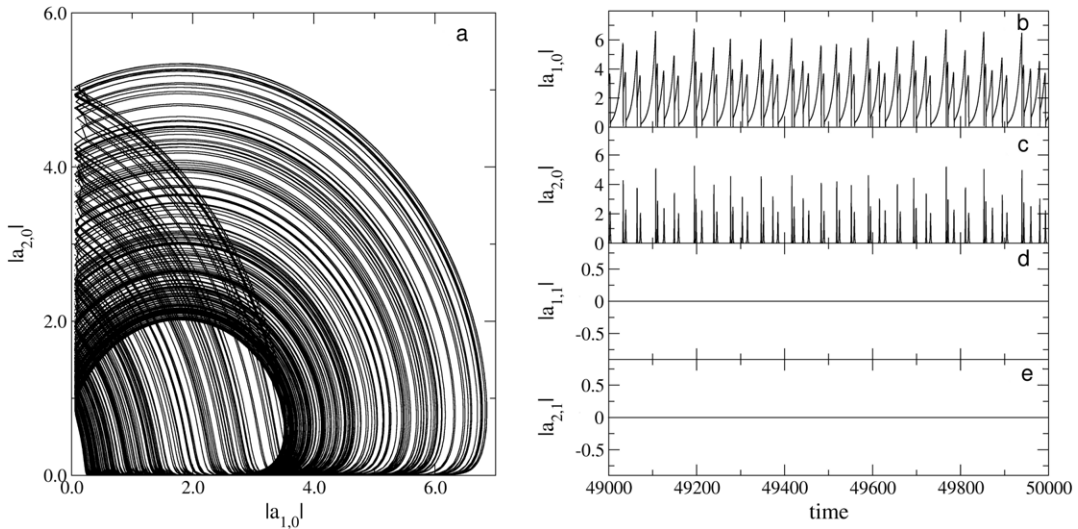


**Fig. 1.** (a) Projection of the low-dimensional attractor in the  $|a_{2,0}|$  vs.  $|a_{1,0}|$  section of the homogeneous manifold, for  $\nu_1 = 0.1, \nu_{2,3} = -1.80$ . (b)–(e) Time evolution of the (Fourier) mode amplitudes  $|a_{\alpha,n}|$  for  $\alpha = 1, 2$  and  $n = 0, 1$ .

numerical simulations. Eqs. (3)–(5) were numerically integrated by a pseudo-spectral method using a fixed number  $N$  of modes in Fourier space [18,17]

$$A_\alpha(x, t) = \sum_{n=-(N/2)+1}^{N/2} |a_{\alpha,n}(t)| \exp\{i[\kappa_{\alpha,n}x + \phi_{\alpha,n}(t)]\}, \quad (\alpha = 1, 2, 3), \tag{6}$$

where  $a_{\alpha,n}(t)$  is the time-dependent Fourier coefficient corresponding to the mode number  $\kappa_{\alpha,n} = 2\pi n/L$ .

The time evolution of the Fourier mode amplitudes is governed by a system of  $6N$  coupled ordinary differential equations, which were integrated using a 12th order Adams predictor–corrector method. We considered, in the numerical simulations, a one-dimensional box of length  $L = 2\pi/\kappa_{1,1} = 2\pi/0.89$ , and with periodic boundary conditions. The initial conditions are chosen as  $F_{1,0}(0) = 0.500 + i0.000$ , and  $F_{2,\pm 1}(0) = 0.001 + i0.001$ , where

$$F_{\alpha,n}(t) = a_{\alpha,n}(t)e^{i\phi_{\alpha,n}(t)}, \tag{7}$$

all the other modes being set to zero.

In the following we shall work in the  $6N$ -dimensional Fourier phase space comprised of the  $N$  complex mode amplitudes  $a_{\alpha,n}, n = 0, 1, 2, \dots, N$ , for each wave  $\alpha = 1, 2, 3$ . This is a highly convenient mathematical description since the modes with  $n = 0$  are purely temporal, and we can investigate the excitation of spatial modes by looking at the  $n \neq 0$  amplitudes. This is done, for example, in Fig. 1(a), where we plot a two-dimensional phase space section with  $|a_{2,0}|$  versus  $|a_{1,0}|$ , i.e. the modulus of the amplitudes for the purely temporal modes of the parent wave and one of its daughters.

The attractor seems chaotic, and indeed it is according to the computed Lyapunov exponent, a feature also suggested by the corresponding time series (Fig. 1(b), (c)). On the other hand, no spatial modes are excited for this value of the control parameter (Fig. 1(d), (e)). At each cycle the parent wave grows exponentially with rate  $\nu_1$ , until its amplitude is so large that nonlinear terms dominate causing saturation, the corresponding energy being imparted to the daughter waves (modes  $|a_{2,0}|$  and  $|a_{3,0}|$ ), which grow rapidly as the parent wave decays, in spike-like events (Fig. 1(c)).

For a different value of the control parameter  $\nu_{2,3}$  the chaotic attractor of the mode  $n = 0$  drives spatial mode excitation, and thus spatio-temporal chaos, as revealed by the bubbling spikes in the spatial mode amplitudes  $|a_{1,1}|$  and  $|a_{2,1}| \neq 0$  (Fig. 2). The spatial modes excited by the chaotic temporal dynamics produce non-homogeneous spatial patterns, as illustrated Fig. 3(a) and (b), where space–time plots of the combination  $|A_2|^2 - |A_3|^2$  are shown corresponding to the same parameter sets used to draw Figs. 1 and 2, respectively.

This particular combination was chosen because it is a constant of motion of the purely temporal system, where the expression  $|A_2|^2 - |A_3|^2 = \text{const.}$  comes from one of the so-called Manley–Rowe conditions [29]. Hence any non-constant behavior of the quantity  $|A_2|^2 - |A_3|^2$  can be assigned to deviations from purely temporal behavior, and thus it is a sensitive diagnostic of spatial mode excitation.

### 3. Transition to spatio-temporal chaos

The dynamics of the purely temporal Fourier mode is determinant on the spatial mode excitation. The general features of the parent wave dynamics are conveyed by the bifurcation diagrams of Fig. 4, where we compare three different values

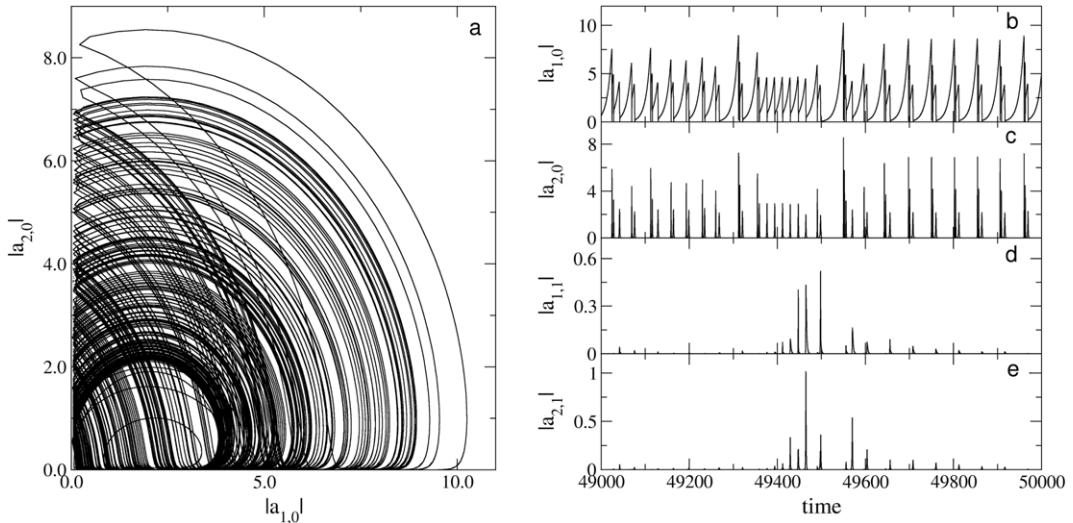


**Fig. 2.** (a) Projection of the low-dimensional attractor in the  $|a_{2,0}|$  vs.  $|a_{1,0}|$  section of the homogeneous manifold, for  $\nu_1 = 0.1$ ,  $\nu_{2,3} = -2.00$ . (b)–(e) Time evolution of the (Fourier) mode amplitudes  $|a_{\alpha,n}|$  for  $\alpha = 1, 2$  and  $n = 0, 1$ .

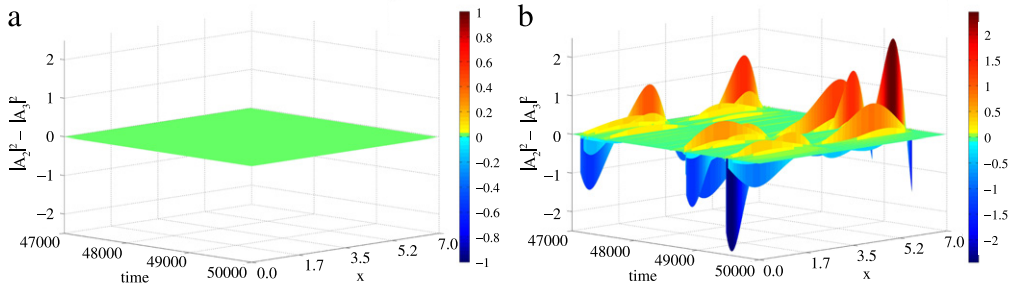


**Fig. 3.** (Color online) Space-time plots of  $|A_2|^2 - |A_3|^2$  for (a)  $\nu_{2,3} = -1.80 > \nu_{CR} = -1.96$ ; (b)  $-2.00 < \nu_{CR}$ .

of the diffusion coefficient (Fig. 4(a)–(c)) with the case of no diffusion at all (Fig. 4(d)) (temporal case only). The similarity among these bifurcation diagrams indicates that the dynamics of the purely temporal mode is not affected noticeably by the diffusion effect. Hence the purely temporal dynamics drives the spatial dynamics in a master-slave unidirectional coupling.

The preliminary analysis of Figs. 1 and 2 suggests a transition to spatio-temporal chaos for  $\nu_{2,3}$  between 1.8 and 2.0 for marking the onset of spatial mode excitation in the system (3)–(5). From the bifurcation diagrams of Fig. 4 this value coincides with the onset of chaos within a periodic window. One of the main points of this work is that a necessary feature for spatial mode excitation is the presence of chaotic dynamics in the purely temporal mode. If the corresponding attractor is periodic, for example, no spatial inhomogeneities are observed.

This strong conclusion needs a careful numerical check, which can be provided by the complex order parameter introduced by Kuramoto [33]

$$z_\alpha(t) = R_\alpha(t) \exp(i\Phi_\alpha(t)) \equiv \frac{1}{N} \sum_{n=-(N/2)+1}^{N/2} \exp(i\varphi_{\alpha,n}(t)), \tag{8}$$

where  $R_\alpha(t)$  and  $\Phi_\alpha(t)$ ,  $\alpha = 1, 2, 3$ , are the amplitude and angle, respectively, of a centroid phase vector for a one-dimensional lattice of Fourier modes with periodic boundary conditions. The phase angle is obtained geometrically from the kind of chaotic attractor that is shown in Figs. 1(a) and 2(a):

$$\varphi_{\alpha,n}(t) = \arctan \left\{ \frac{\text{Im}[a_{\alpha,n}(t)]}{\text{Re}[a_{\alpha,n}(t)]} \right\}. \tag{9}$$

We compute the average of the order parameter magnitude  $\overline{R_\alpha}$  over a time interval large enough to warrant that an asymptotic state has been achieved by the system. This is a reliable diagnostic of spatial mode excitation, since if we have purely temporal dynamics all spatial mode numbers have amplitudes equal to zero. In terms of the centroid phase vectors defined by (9) we have a coherent superposition yielding  $\overline{R_\alpha} = 1$ , or a perfectly coherent and homogeneous state [34]. On the other hand, once some spatial modes are excited the order parameter decreases, such that the transition to spatio-temporal

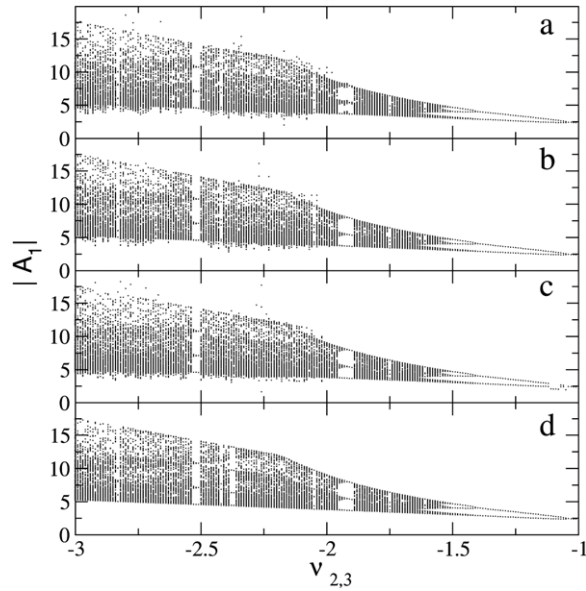


**Fig. 4.** Bifurcation diagram for the amplitude of the parent wave vs. the decay rate of the daughter waves for different values of the diffusion coefficient: (a)  $D = 1.5$ ; (b) 1.0; (c) 0.6; and (d) no diffusion (temporal case only).

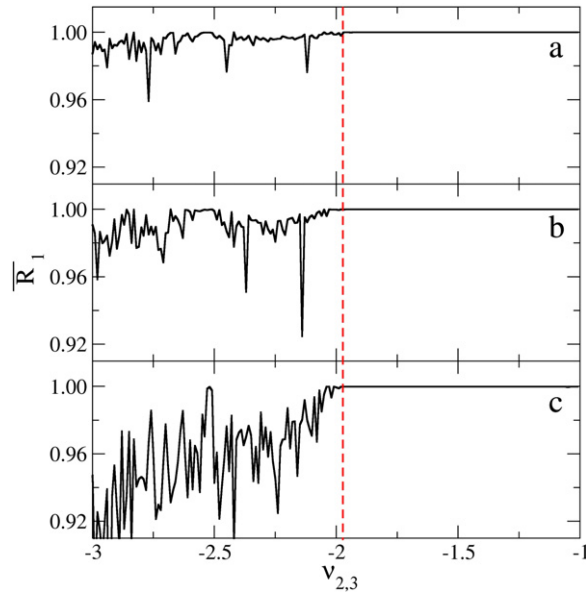


**Fig. 5.** Average order parameter magnitude (for the parent wave dynamics) as a function of the decay rate of the daughter waves for different values of the diffusion coefficient: (a)  $D = 1.5$ ; (b) 1.0; and (c) 0.6. The dashed line indicates the transition to spatio-temporal chaos.

chaos is the point where  $\overline{R}_\alpha$  becomes different from unity. The results of such analysis are in Fig. 5 for different values of the diffusion coefficient.

Confirming our initial guess that spatial diffusion do not affect noticeably the purely temporal dynamics, we observe in Fig. 5(a)–(c) that the transition from purely temporal dynamics to spatio-temporal chaos occurs at the critical value  $\nu_{2,3} = \nu_{CR} = -1.96$  for different values of the diffusion coefficient (represented as a dashed line in Fig. 5).

**4. Lyapunov exponent analysis**

We can use the language of Fourier phase space to unravel some details of this transition, such as the type of bifurcation (if any) and how could be the general characteristics of it which would be also present in other spatially extended system. Using the Fourier phase space description, the  $\kappa_{\alpha,0} \neq 0$  modes, with  $\alpha = 1, 2, 3$  are purely temporal (with periodic, quasi-

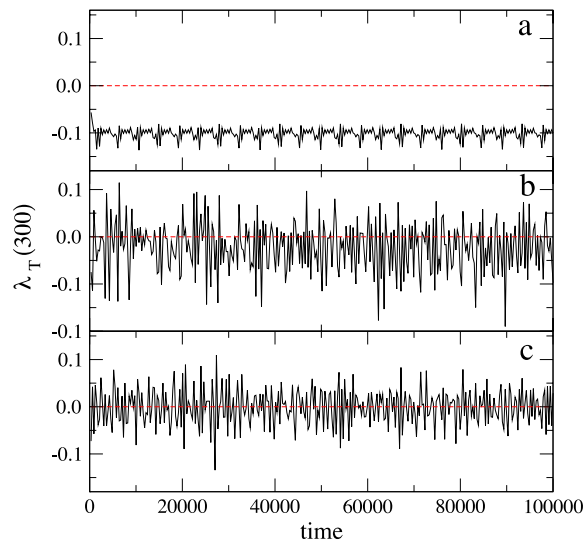


**Fig. 6.** Time series for the time-300 maximal transversal Lyapunov exponent for different values of the decay rate of the daughter waves: (a)  $\nu_{2,3} = 1.5$ ; (b)  $-1.8$ ; (c)  $-2.0$ .

periodic, or chaotic dynamics) and a spatially homogeneous state. The latter defines a three-dimensional subspace called homogeneous manifold  $\mathcal{M}$ , embedded in the  $6N$ -dimensional Fourier phase space. For the case  $\nu_2 = \nu_3$ , and thanks to a phase conjugacy in Eqs. (3)–(5), it is possible to show that the homogeneous manifold is invariant with respect to the system dynamics: once an initial condition is placed there, the ensuing trajectory remains in  $\mathcal{M}$  for all further times under the dynamics generated by the  $\kappa_{\alpha,0}$  modes. Accordingly, the spatially inhomogeneous modes  $\kappa_{\alpha,n}$  are related to the remaining  $3(2N - 1)$  directions transversal to  $\mathcal{M}$ .

In this framework we can compute the Lyapunov spectrum related to the mode dynamics in the Fourier phase space. Since each Fourier mode for the three interacting waves is a degree of freedom in this space, the spectrum can be computed from  $6N$  Lyapunov exponents, using Gram–Schmidt reorthonormalization [35,36]. Since the homogeneous manifold is three-dimensional, three of the Lyapunov exponents (out of  $6N$  modes considered) are such that the greatest is positive, the other being equal to zero and negative, related to the chaotic attractor which belongs to the homogeneous manifold. From the remaining  $6N - 3$  transversal Lyapunov exponents we are particularly interested in the largest one, which we shall denote as  $\lambda_T$  and call *maximal transversal exponent*. Hence the transition from purely temporal chaos to spatial mode excitation occurs when  $\lambda_T = 0$ , going from negative to positive values. This analysis have confirmed our critical value of  $\nu_{CR} = -1.96$  for the transition point.

However, other information can be obtained from a detailed examination of the largest transversal exponent, particularly its fluctuations. The latter are quantified by the time- $t$  maximal transversal Lyapunov exponents  $\lambda_T(t)$ , which are computed from the same principles as the usual exponents, but using a finite (and usually small) value of  $t$ . Since the actual value of  $\lambda_T(t)$  depends on the initial condition we consider a random sample of initial conditions outside the homogeneous manifold and compute the value of  $\lambda_T(t)$  for each initial condition. Actually, we use the recurrency of dynamics and follow a single trajectory a large number of steps. The time- $t$  exponents are then computed from consecutive and non-overlapping length- $t$  sections of the trajectory. Our results are in Fig. 6, where we show the time evolution of the time-300 maximal transversal Lyapunov exponent  $\lambda_T(300)$ . Long before the transition to spatial mode excitation (Fig. 6(a)) all values of  $\lambda_T(300)$  are negative, and so their mean value, as expected since we do not have spatial modes excited for this value of the control parameter.

Now if we look to the vicinity of the transition point  $\nu_{CR}$  things are not so simple. Before (Fig. 6(b)) and after (Fig. 6(c)) the transition the fluctuations of  $\lambda_T(300)$  look the same: they both have positive and negative fluctuations as well. The difference between such cases is in the average value of the exponent, it is negative just before the transition (Fig. 6(b)) and positive just after (Fig. 6(c)). However, the presence of positive fluctuations of  $\lambda_T(300)$  before the transition is counter-intuitive, since the fluctuation reflect local expansion or contraction rates in phase space and thus positive fluctuations would mean spatial mode spikes. These spikes represent trajectories which deviate from the homogeneous manifold along some transversal directions in the Fourier phase space. But since the average Lyapunov exponent is negative, these excursions are exponentially damped and are actually transient phenomena. After the transition to spatio-temporal chaos, on the other hand, the average Lyapunov exponent becomes positive, and the spatial mode spikes become permanent.

A systematic way to quantify the difference between transient and permanent behavior of spatial mode spikes is to compute the probability distribution function for the time-300 maximal transversal Lyapunov exponent, which we denote as  $P[\lambda_T(300)]$ , such that  $P[\lambda_T(300)]d\lambda_T(300)$  is the number of time-300 maximal transversal Lyapunov exponents between  $\lambda_T(300)$  and  $\lambda_T(300) + d\lambda_T(300)$  [37]. In Fig. 7 we show numerical approximations of this probability distribution function.

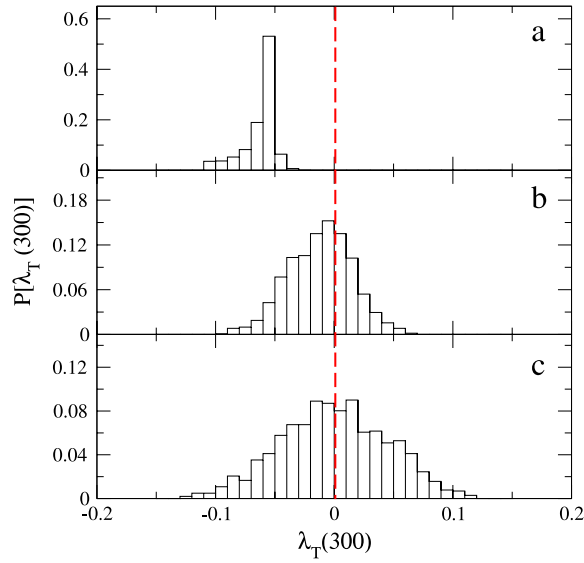


**Fig. 7.** Probability distribution function of the time-300 maximal transversal Lyapunov exponent for different values of the decay rate of the daughter waves: (a)  $\nu_{2,3} = 1.5$ ; (b)  $-1.8$ ; (c)  $-2.0$ .

In fact, for  $\nu_{2,3}$  far enough from the transition point  $\nu_{CR}$  all the finite-time transversal exponents are negative (Fig. 7(a)), as well as their average

$$\langle \lambda_T(t) \rangle = \int_{-\infty}^{+\infty} \lambda_T(t) P[\lambda_T(t)] d\lambda_T(t), \quad (10)$$

provided the distribution is normalized to the unity

$$\int_{-\infty}^{+\infty} P[\lambda_T(t)] d\lambda_T(t) = 1. \quad (11)$$

Just before the transition to turbulence at  $\nu_{CR}$  the probability distribution function gains positive values (Fig. 7(b)) and thus the fraction of positive time- $t$  exponents

$$\phi[\lambda_T(t)] = \int_0^{\infty} P[\lambda_T(t)] d\lambda_T(t) \quad (12)$$

becomes positive. Just after the transition (Fig. 7(c)) the positive fraction has further increased. The blowout bifurcation occurs just as the positive fraction is equal to 1/2, i.e. exactly half of the time- $t$  exponents are positive [38].

The variation of the positive fraction of exponents with the control parameter is depicted in Fig. 8(a), along with the average value of them given by Eq. (10) (cf. Fig. 8(b)). In Fig. 8(c) we show for comparison the bifurcation diagram of the modulus of the parent mode amplitude. One noteworthy feature is that the control parameter values that yield spatio-temporal chaos (i.e. nonzero values of  $\phi[\lambda_T(t)]$ ) always correspond to a chaotic behavior of the parent wave. For example, at  $\nu = -1.75$ , since we are within a periodic window there should be no spatial mode excitation and hence  $\phi$  should be zero there (the small value we found in Fig. 8(a) is due to numerical errors, since we are too close to a bifurcation, where transients are quite long yielding a slow convergence of Lyapunov exponents). This reinforces our previous observation that chaos in the homogeneous manifold is a necessary condition for spatial mode excitation.

In addition, the blowout bifurcation points ( $\phi = 1/2$ ) coincide with those points for which the average value of the time- $t$  exponents is zero. This is not surprising, though, since it can be proved that, for  $t$  sufficiently large, the average time- $t$  exponent is also the infinite-time Lyapunov exponent, or

$$\langle \lambda_T(t) \rangle = \lambda_T. \quad (13)$$

A compelling argument in favour of this claim is that, the probability distribution function being Gaussian-like, its maximum is also the average value, and the maximum tends to the infinite-time exponent: if  $t$  goes to infinity, the distribution becomes a delta function centred at  $\lambda_T$ .

Moreover, the blowout bifurcation points are also critical points for crises in the behavior of  $|A_1|$ . This is an interesting feature since, once the chaotic attractor loses transversal stability, it actually becomes a chaotic saddle. And an interior crisis occurs when a chaotic attractor collides with an unstable periodic orbit, becoming a non-attracting chaotic saddle. This crisis can also be inferred from the bifurcation diagram of the parent wave amplitude: a periodic window arises out of a

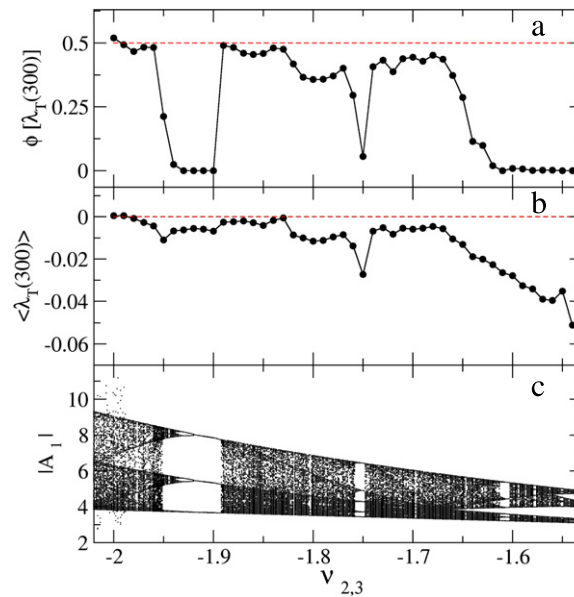


**Fig. 8.** Variation with the decay rate of the daughter waves of the following quantities: (a) Positive fraction of time-300 maximal transversal Lyapunov exponents; (b) average value of the exponents; (c) modulus of the parent mode amplitude.

chaotic attractor from a saddle–node bifurcation which creates two periodic orbits: a stable and an unstable one. The stable orbit bifurcates through a period-doubling cascade and generates a smaller chaotic attractor in the main periodic window. However, this smaller chaotic attractor eventually collides with the unstable periodic orbit generated at the beginning of the window. When they collide – an interior crisis – the smaller chaotic orbit is substantially enlarged. In the bifurcation diagram the generation of a chaotic saddle is very difficult to be distinguished from a chaotic attractor: a trajectory that begins near a chaotic saddle will wander chaotically through the saddle before being repelled from it. However, in Fig. 8(c) the presence of a chaotic saddle (for which  $\phi > 0$ ) is inferred from the added points to the otherwise chaotic attractor.

## 5. Conclusions

Many spatially extended dynamical systems experience a transition to turbulence different from the Ruelle–Takens scenario. In such systems, there is an invariant homogeneous manifold where a chaotic attractor is necessary to fuel the excitation of spatial modes, which are trajectories transversal to this manifold. Chaotic systems with a diffusive coupling may belong to this class if the spatially homogeneous state is actually a solution of the spatially extended system, the solution depending entirely on the purely temporal dynamics on this homogeneous manifold.

In this work we showed that the bubbling transition to turbulence in this class of spatially extended system is due to a blowout bifurcation, whereby the chaotic attractor which drives the spatial mode excitation loses transversal stability and becomes a non-attracting chaotic saddle. We show numerical evidences for this general phenomenon by considering, as a representative example, the nonlinear three-wave interaction with diffusive coupling and group velocities.

We characterized the transition to turbulence with help of an order parameter which has values less than the unity after the transition occurs. The value obtained is compatible with the Lyapunov analysis we have performed. The blowout bifurcation happens when the maximal Lyapunov exponent in the transversal direction is zero. Moreover, the finite-time estimates of this exponent (local contraction or expansion rates) also furnish useful information. The positive values, for example, are related to the spikes observed just before and after the blowout bifurcation. The existence of those spikes is ultimately the cause of this transition being called a bubbling one. Also the blowout bifurcation can be assigned to a crisis in the homogeneous manifold, in which a chaotic attractor becomes a chaotic saddle by its collision with an unstable periodic orbit. This can also explain why the spikes of spatial mode excitation have an intermittent behavior.

## Acknowledgements

This work was made possible by partial financial support of CNEN (Brazilian Fusion Network), CNPq, CAPES, FAPESP, and Fundação Araucária (Brazilian Government Agencies).

## References

- [1] D. Ruelle, F. Takens, *Comm. Math. Phys.* 20 (1971) 167.
- [2] S. Newhouse, D. Ruelle, F. Takens, *Comm. Math. Phys.* 64 (1978) 35.

- [3] P. Manneville, *Instabilities, Chaos And Turbulence: An Introduction To Nonlinear Dynamics And Complex Systems*, Imperial College Press, London, 2004.
- [4] L.A. Bunimovich, Ya.G. Sinai, *Nonlinearity* 1 (1988) 491.
- [5] J. Bricmont, A. Kupiainen, *Physica D* 103 (1997) 18.
- [6] M. Jiang, Y.B. Pesin, *Comm. Math. Phys.* 193 (1998) 675.
- [7] B. Fornberg, *A Practical Guide to Pseudospectral Methods*, Cambridge University Press, Cambridge, 1996.
- [8] U. Frisch, *Turbulence: The Legacy of A.N. Kolmogorov*, Cambridge University Press, Cambridge, 1995.
- [9] J.C.P. Coninck, S.R. Lopes, R.L. Viana, *Phys. Rev. E* 70 (2004) 56403.
- [10] J.C.P. Coninck, S.R. Lopes, R.L. Viana, *Physica A* 343 (2004) 247.
- [11] K. He, A.C.-L. Chian, *Phys. Rev. Lett.* 91 (2003) 034102.
- [12] K. He, *Phys. Rev. Lett.* 94 (2005) 034101.
- [13] C. Grebogi, E. Ott, J.A. Yorke, *Phys. Rev. A* 37 (1988) 1711.
- [14] P. Ashwin, J. Buescu, I. Stewart, *Phys. Lett. A* 193 (1994) 126.
- [15] S.C. Venkataramani, B.R. Hunt, E. Ott, D.J. Gauthier, J.C. Bienfang, *Phys. Rev. Lett.* 77 (1996) 5361.
- [16] S.C. Venkataramani, B.R. Hunt, E. Ott, *Phys. Rev. E* 54 (1996) 1346.
- [17] J.D. Szezech Jr., S.R. Lopes, R.L. Viana, *Phys. Rev. E* 75 (2007) 067202.
- [18] J.D. Szezech Jr., S.R. Lopes, R.L. Viana, I.L. Caldas, *Physica D* 238 (2009) 516.
- [19] E. Covas, P. Ashwin, R. Tavakol, *Phys. Rev. E* 56 (1997) 6451.
- [20] P.P. Galuzio, S.R. Lopes, R.L. Viana, *Phys. Rev. Lett.* 105 (2010) 055001.
- [21] E. Ott, J.C. Sommerer, *Phys. Lett. A* 188 (1994) 39.
- [22] L. Turner, *Phys. Rev. E* 54 (1996) 5822.
- [23] Y.C. Li, *Int. J. Bifurcat. Chaos* 17 (2007) 85.
- [24] A.C.-L. Chian, S.R. Lopes, M.V. Alves, *Astron. Astrophys.* 290 (1994) L13.
- [25] A.C.-L. Chian, F.B. Rizzato, *J. Plas. Phys.* 51 (1994) 61.
- [26] A. Rundquist, C.G. Durfee UU, Z. Chang, C. Heine, S. Backus, M.M. Murname, H.C. Kapteyn, *Science* 280 (1998) 1412.
- [27] G.I. Stegeman, M. Segev, *Science* 286 (1999) 1518.
- [28] A. Picozzi, M. Haeltermann, *Phys. Rev. Lett.* 86 (2001) 2010.
- [29] D.J. Kaup, A. Reiman, A. Bers, *Rev. Modern Phys.* 51 (1979) 275.
- [30] C.C. Chow, A. Bers, A.K. Ram, *Phys. Rev. Lett.* 68 (1992) 3379.
- [31] S.R. Lopes, F.B. Rizzato, *Phys. Rev. E* 60 (1999) 5375.
- [32] M. Frichembruder, R. Pakter, F.B. Rizzato, *Physica D* 215 (2006) 99.
- [33] Y. Kuramoto, *Chemical Oscillations, Waves, and Turbulence*, Springer Verlag, Berlin, 1984.
- [34] S.E. de, S. Pinto, S.R. Lopes, R.L. Viana, *Physica A* 303 (2002) 339.
- [35] A. Wolf, J.B. Swift, H.L. Swinney, J.A. Vastano, *Physica D* 16 (1985) 285.
- [36] M. Yamada, K. Ohkitani, *Phys. Rev. Lett.* 60 (1988) 983.
- [37] J. Aguirre, R.L. Viana, M.A.F. Sanjuán, *Rev. Modern Phys.* 81 (2009) 333.
- [38] R.L. Viana, C. Grebogi, S.E. de, S. Pinto, S.R. Lopes, A.M. Batista, J. Kurths, *Physica D* 206 (2005) 94.